The Role of Materials and Defects on the Electroforming of Metal/Oxide/Metal Stacks *(Invited)*

Stephan Menzel *(IEEE Senior Member)*
Peter-Grünberg-Institut (PGI-7)
Forschungszentrum Jülich GmbH
Jülich, Germany
+492461615339, e-mail address: st.menzel@fz-juelich.de

Nils Kopperberg
Institut für Werkstoffe der Elektrotechnik II (IWE2)
RWTH Aachen University
Aachen, Germany

***Abstract*— Soft dielectric breakdown, i.e., electroforming, of metal/oxide/metal stacks leads to a local reduction of the oxide in a filamentary region. This process is required to operate filamentary RRAM devices thereafter. In this work, different parameters influencing the electroforming process are investigated using simulations. The parameters studied are the role of the electrode materials, an initial sub-stoichiometry of the oxide, the applied voltage amplitude, and the ambient temperature. To this end, a 2D axisymmetric physical continuum model and a 3D KMC model are employed. The simulation results are discussed in context of experimental literature data.**

***Index Terms*—Dielectric breakdown, Electroforming, Gate Stack, Modeling, Resistive RAM,**

I. INTRODUCTION

Oxide thin films are widely used in electronic devices. They are used in transistor gate stacks, in dielectric capacitors or as functional layers in resistive random-access memories (RRAMs). Though oxides are highly insulating materials, they may degrade under high electric fields leading to dielectric breakdown. While this effect leads to permanent failure of gate stacks and dielectric capacitors, a so-called soft breakdown is required as initial process to operate RRAMs thereafter [1]. In context with RRAMs this process is called electroforming process as it requires the application of electric fields to form the device. The dielectric breakdown mechanism of the metal/oxide/metal stack is based on the reduction of the oxide material, e.g., HfO_2, Ta_2O_5, ZrO_2, and the formation of filamentary conductive path within the oxide material short-circuiting the metal electrodes. First studies defined a critical electrical field that induces the dielectric breakdown, which is a property of the oxide material solely [2]. Later it was shown that other factors such as initial oxide stoichiometry, electrode materials, or moisture influence the electroforming voltage as well [3], [4], [5], [6].

In this work, different factors influencing the electroforming process of metal/oxide/metal stacks will be discussed. The paper is organized as follows. First the physics of the electroforming process is discussed. Then, the simulation models of the electroforming process are introduced. Based on the simulation results, the influence of interface properties, ambient conditions, and defect configuration will be discussed in the following sections.

II. PHYSICS OF THE ELECTROFORMING PROCESS

The electroforming process is initiated by applying a high voltage to the metal/oxide/metal stack. The voltage amplitude and pulse length vary strongly from system to system. Whereas dc-voltages need to be applied over a considerable time for thick films or single crystals, the forming takes place in a first switching cycle with moderate voltages for devices with thin oxide films. Various experiments showed the formation of oxygen vacancies during the electroforming process. It was demonstrated that oxygen is released by anodic oxidation, which can occur by the oxidation of an oxidizable electrode material (e.g., Ta, Hf, Ti) or by the release of oxygen gas at an inert electrode [7], [8], [9], [10]. The release of oxygen leads to the formation of positively charged oxygen vacancies at the corresponding interface within the oxide film. These vacancies can move within the applied electric field and further oxygen can be released at the interface [1]. Due to local inhomogeneities and positive feedback mechanism, this leads to the formation of filamentary, reduced oxide regions showing a high number of oxygen vacancies. This may even lead to phase transformations [11], [12], though this may only by a side effect and not necessary to create a conducting filament. For the most common RRAM materials, the oxygen deficiency leads to an increase of local conductivity, either by inducing trap states for trap-assisted tunneling processes or by acting as donors if the induced defects states are shallow [13], [14]. It should be noted that most likely the formation not only happens at one location but a several ones and one filament wins [15], [16].

The electroforming process typically happens at higher voltages than the typical switching voltages of RRAMs. This is

---

This work was supported by the Federal Ministry of Education and Research (BMBF, Germany) as part of the project NEUROTEC II (16ME0398K, 16ME0399)

critical as often specific transistors are required for co-integration with CMOS. It also limits the integration of RRAM technology with smaller CMOS nodes. Thus, for RRAM application it is favorable to reduce the forming voltage to the range of the switching voltages. In contrast, the forming/breakdown voltage needs to be increased for application of metal/oxide/metal films for DRAM or gate stack applications. Thus, it is important to understand the physical parameters that determine the forming voltage, which is partially addressed in this work using device simulation.

III. SIMULATION METHODS

In this work, two different simulation methods are applied to simulate the electroforming process. First, we use a continuum model based on solving drift-diffusion equations. This allows us to study trends of material parameters. To account for the stochasticity of the underlying processes and the fact that a low number of defects are present in the early stages of the electroforming, a Kinetic Model Carlo (KMC) model is employed. While the latter method offers the possibility to study atomistic processes, the long simulation time and the limited size of the solution time restricts this approach. In contrast, the continuum method enables the simulation of larger domains which is important for modeling the heat dissipation. Moreover, parametric studies can be easily performed and analyzed. In the case of KMC models many simulations need to be performed per parameter to avoid statistical effects. Both models are based on the physical model of the electroforming process discussed in the previous section including oxygen exchange reactions, oxygen vacancy migration, and Joule heating.

A. Kinetic Monte Carlo Model

The 3D Kinetic Monte Carlo (KMC) simulation model utilized in this study is based on the foundational work by Abbaspour *et al.* [17] and was first published in its current form in [18] by Kopperberg *et al.*. This model is specifically designed to simulate the stochastic processes governing oxygen vacancy (Vö) dynamics within the oxide layer of valence change memory (VCM) RRAM devices. It enables detailed analysis of forming and resistive switching by accounting for key atomic-scale processes, including generation, diffusion, and recombination of oxygen vacancies.

The simulation operates on a cubic lattice structure with a spacing of 0.5 nm between lattice points, representing a 6 x 6 x 6 nm³ HfO_x layer sandwiched between two metal electrodes. The model incorporates a range of physical phenomena, including the influence of electric fields, local potential variations, and thermal effects on oxygen vacancy dynamics. Poisson's equation is solved to compute the electric potential, which reflects the combined influence of an applied voltage and the space charge within the material. The current through the oxide layer is determined using a trap-assisted tunnelling (TAT) solver, which is particularly suitable for describing conduction in the high-resistance state (HRS). For further details on the TAT mechanism, see [18] and related studies.

A distinguishing feature of the model is the inclusion of diffusion-limiting domains, introduced in [18]. These domains divide the oxide layer into cubic sub-regions where oxygen vacancy diffusion is characterized by distinct energy barriers. Inside a domain, oxygen vacancy diffusion occurs relatively easily, with an activation energy of $E_D = 0.7$ eV. In contrast, transitions between domains encounter a higher energy barrier of $E'_D = 1.2$ eV, reflecting the hindered mobility at domain boundaries. This refinement allows the model to replicate both short-term variability and long-term retention effects, which are crucial for understanding forming and stability in VCM devices.

The transition rates for Vö generation (R_G), diffusion (R_D), and recombination (R_R) are calculated using Transition State Theory (TST):

$$R_{G/D/R} = \nu_0 \exp\left(-\frac{E_{G/D/R} - q\Delta\phi}{k_B T}\right), \tag{1}$$

where ν_0 is the attempt frequency, $E_{G/D/R}$ denotes the activation energy for generation, diffusion, or recombination, $q = +2e$ is the charge of an oxygen vacancy, and $\Delta\Phi$ is the potential difference between adjacent lattice sites. Diffusion and generation, the dominant processes during forming, are driven by local electric fields and thermal activation. In contrast, recombination of oxygen vacancies, although included in the model, plays a negligible role under forming conditions due to the polarity of the applied voltage, which favors oxygen vacancy generation and diffusion.

The KMC algorithm iteratively evaluates all possible transitions in the system, selects one process based on weighted probabilities, and updates the simulation state and time. At each simulation step, the time increment Δt is determined based on the total transition rate $R_{\mathrm{tot}} = \sum_i R_i$ using:

$$\Delta t = -\frac{\ln(r)}{R_{\mathrm{tot}}} \tag{2}$$

where r is a uniformly distributed random number in the interval (0,1]. The simulation time is updated as $t = t + \Delta t$. This stochastic approach captures the inherent variability in Vö dynamics, which is critical for modelling the forming process in VCM devices.

Overall, the 3D KMC model provides a robust framework for investigating the forming process by capturing the interplay between Vö dynamics, electric fields, and structural features such as diffusion-limiting domains. Further details on the model, its implementation, and previous results can be found in [18] and [19].

B. Continuum Model

The continuum model is based on the drift-diffusion approach presented to study the RESET dynamics of TaO_x-based resistive switches [20], and then extended to include the kinetics of oxygen exchange at the electrodes to simulate the electroforming process [21]. The model geometry consists of a 2D axisymmetric representation with radius $R = 100$ nm of a metal-oxide-metal structure on a substrate carrier. The electronic carrier transport is modelled by a drift-diffusion model assuming electron transport in the conduction band and injection/ejection of electrons at the two metal/oxide interfaces over/through a Schottky-like barrier. Due to the high self-doping by oxygen vacancies the transport is mainly due to electron tunneling [14], [22]. In the model a high Schottky-barrier is assumed in contact with high work function metal at the bottom electrode, whereas an ohmic contact is assumed at the interface between the oxide layer and the low work function, top metal electrode.

The set of equations to simulate the electroforming process is discussed in our previous work [20], [21]. The model relies on the coupled electronic-ionic transport under non-isothermal conditions by calculating the self-consistent steady-state solution of the heat equation, Poisson equation and electron drift-diffusion equation, followed by the calculation of a time step for oxygen-vacancy movement by solving the drift-diffusion equation for doubly ionized oxygen vacancies and the rate equations for the singly ionized and neutral vacancies. To account for the effects of contact potential, electron transport across the interface barrier via thermionic emission and tunneling is included in the model. In the following, the ionic model of the oxygen exchange is introduced as published in [21].

To introduce oxygen vacancies to the oxide system, oxygen release and incorporation is accounted for at the Schottky-like electrode/oxide interface, while the ohmic electrode interface is assumed to block the ionic current. The oxygen-exchange reaction is assumed to take place in a confined region $r \leq r_{\mathrm{fil}}$ at the bottom electrode interface. It is modeled using a Butler-Volmer equation for the oxygen-vacancy current density J_{VO} as boundary condition for the oxygen-vacancy drift-diffusion equation according to

$$\begin{aligned} J_{\mathrm{VO}}(r,0) = {} & J_0(r,0) \cdot S(r) \cdot \\ & \left[\frac{N_{\mathrm{VO,M}}(r,0)\, N_{\mathrm{O,SC}}(r,0)}{N^*_{\mathrm{VO,M}} N^*_{\mathrm{O,SC}}} \exp\left(-\frac{\alpha z_{\mathrm{VO}} e}{k_{\mathrm{B}} T} \Delta\eta \right) \right. \\ & \left. - \frac{N_{\mathrm{O,M}}(r,0)\, N_{\mathrm{VO,SC}}(r,0)}{N^*_{\mathrm{O,M}} N^*_{\mathrm{VO,SC}}} \exp\left(\frac{(1-\alpha) z_{\mathrm{VO}} e}{k_{\mathrm{B}} T} \Delta\eta \right) \right]. \end{aligned} \tag{3}$$

Here, J_0 is the exchange current density, $N_{\mathrm{O,SC}}$ ($N_{\mathrm{VO,SC}}$) is the oxygen ion (vacancy) concentration in the oxide layer, $N_{\mathrm{O,M}}$ and $N_{\mathrm{VO,M}}$ are oxygen-defect concentrations in the metal electrode, $N_{\mathrm{O,SC}}^*$, $N_{\mathrm{VO,SC}}^*$, $N_{\mathrm{O,M}}^*$, and $N_{\mathrm{VO,M}}^*$ are corresponding reference concentration values, α is the transfer coefficient, z_{VO} is the number of involved electrons, k_{B} is the Boltzmann constant, T is the temperature, and $\Delta\eta$ is the overpotential driving the reaction. The latter can be calculated from the difference between the metal Fermi level $E_{\mathrm{F,M}}$ and the electron quasi-Fermi level in the oxide $E_{\mathrm{Fn,SC}}$ according to

$$\Delta\eta = \frac{1}{e}\left(E_{\mathrm{F,M}} - E_{\mathrm{Fn,SC}} \right). \tag{4}$$

The exchange current density can be expressed as

$$J_0(r,0) = z_{\mathrm{VO}} e k_{00} \exp\left(\frac{-\Delta G^\circ}{k_{\mathrm{B}} T} \right) \cdot \frac{\left(N^*_{\mathrm{VO,M}} N^*_{\mathrm{O,SC}} \right)^{1-\alpha}}{\left(N^*_{\mathrm{O,M}} N^*_{\mathrm{VO,SC}} \right)^{-\alpha}} \tag{5}$$

with k_{00} being the reaction-rate constant and ΔG° the Gibbs free energy of activation under standard conditions. The logistic function $S(r)$ is used to produce a smooth decrease of the exchange current density around $r = r_{\mathrm{fil}}$. During the electroforming process, oxygen is transferred from oxide to the metal electrode, which is treated to act as an oxygen reservoir that can receive and release oxygen ions. Neglecting thermodiffusion, and the voltage drop across the electrode, the oxygen-ion distribution in the electrode is simulated by solving the diffusion equation for oxygen ions

$$\frac{\partial N_{\mathrm{O,M}}}{\partial t} = -\frac{1}{z_{\mathrm{O}} e} \nabla \cdot J_{\mathrm{O}} = \nabla \cdot \left(D_{\mathrm{O}} \nabla N_{\mathrm{O,M}} \right). \tag{6}$$

Here, J_{O} denotes the oxygen-ion current density, z_{O} denotes the charge number and D_{O} the diffusion coefficient. The ionic flux at the oxide boundary is opposite to the vacancy flux given by (1) and thus obeys

$$J_{\mathrm{O}}(r,0) = -J_{\mathrm{VO}}(r,0). \tag{7}$$

No oxygen exchange is assumed to take place with the surrounding atmosphere, i.e. $J_{\mathrm{O}}(r, z = -25\ \mathrm{nm}) = 0$.

IV. ELECTROFORMING UNDER CONSTANT VOLTAGE STRESS

Simulations of the electroforming procedure using the continuum model are conducted under constant voltage stress. Initially, a homogeneous donor concentration $N_{\mathrm{VO}} = 1\times10^{16}\ \mathrm{cm}^{-3}$ is assumed in the oxide layer, and no oxygen ions are assumed to be present in the Schottky-like electrode. A constant voltage pulse with varying amplitude and a rise time of 1 ns is applied to the device, and the simulation is stopped after a current increase to 300 µA or more has been achieved. Figure 1(a) shows the simulated *I-t* characteristics and (b) the corresponding average oxygen vacancy concentrations along the rotation axis for the voltage amplitudes of 1.5 V to 3.5 V in 0.5 V steps. All current transients show a plateau-like regime and a succeeding steep current increase. Comparing the current transients to the change in the average oxygen vacancy concentration reveals that oxygen exchange already happens while the current is not changing much. The increase in current is related to the continuous increase in oxygen-vacancy concentration in the oxide layer, which is shown in Fig. 1(b). The onset of the steep current increase can be related to a positive feedback mechanism due to Joule heating. As soon as Joule heating sets in, an increase in the average oxygen concentration will not only lead to an increase in current, but also to an increase in local temperature. The ionic transport as well as the oxygen exchange are temperature activated processes. Thus, an increase in temperature leads to an acceleration of the ion movement and the oxygen exchange rate, which speeds up the transition further leading to a runaway process. Moreover, the time of the onset of the current increase changes orders of magnitude when changing the voltage, which is consistent with experimental findings [23].

Another interesting aspect is revealed when investigating oxygen vacancy distribution during the electroforming process as shown in Fig. 1(c). Though the current increases for both voltage cases, the evolution of the oxygen vacancy distribution differs strongly. The concentration maps show the evolution of

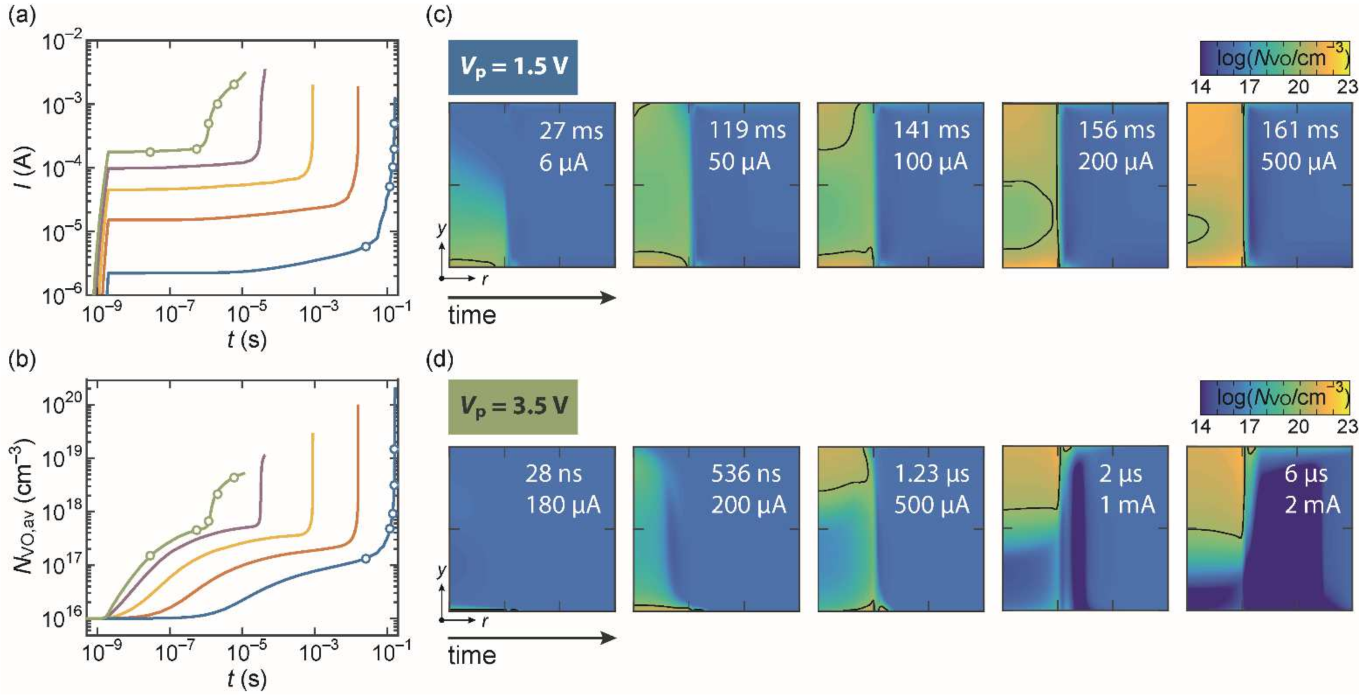

Figure 1. Simulated (a) I-t characteristics and (b) $N_{VO,av}$-t characterstics under constant voltage stress of V_P = {1.5 V, 2 V, 2.5 V, 3 V, 3.5 V} applied to the bottom electrode of the deviceEvolution of the total oxygen vacancy concentration over time for(c) V_P = 1.5 V and (d) V_P = 3.5 V. The snapshots correspond to the open circles in (a) and (b). The black line in the concentration maps (c), (d) marks the isoline $N_{VO} = 1\cdot10^{20}$ cm^{-3} of illustrates the filament evolution.

the distribution from the symmetry axis outwards within the oxide layer. The oxygen exchange happens at the bottom electrode in a region $0 \leq r \leq 10$ nm (marked with a black tick). For V_P = 1.5 V, the oxygen vacancies generated at the bottom electrode interface via the oxygen exchange reaction migrate only slowly towards the top interface. There is always a high concentration of oxygen vacancies (indicative by the green color) at the bottom interface. Thus, one can consider the filament to grow from the bottom electrode towards the top electrode though the growth is more complex when tracing the isoline of $N_{VO} = 1\cdot10^{20}$ cm^{-3}. In contrast, the oxygen vacancy concentration gets depleted during the electroforming process for V_P = 3.5 V. In this case, the filament grows from the top electrode to the bottom electrode.

The different growth modes can be understood as interplay of the rate of the oxygen transfer reaction a the bottom electrode supplying oxygen vacancies and the rate of oxygen vacancy migration [21]. If the exchange rate is high compared to the migration rate, there is always a high concentration of oxygen vacancies at the bottom electrode and the filament grows from bottom to top. In the opposite case, the generated oxygen vacancies rapidly migrate to the top where they accumulate. Thus, the oxygen vacancy concentration gets depleted and the filament grows from top to bottom. In the present simulation study, the relation between the two rates change as the migration and the oxygen exchange have different voltage dependence and temperature dependence. At low voltages, the oxygen transfer is faster than the ion migration and vice versa for high voltages. In addition, the temperature is non-homogenous and lower at the boundaries than the middle of the cell. Thus, the oxygen exchange shows a weaker temperature acceleration than the oxygen migration.

The occurrence of the different growth directions have been experimentally observed in literature [8], [15], [24]. Filaments can grow from the cathode or the anode, depending on factors such as the electrode material, oxygen exchange layers, and the polarity of the forming voltage. While Yalon *et al.* [24] demonstrated that electrode chemistry strongly influences the direction; Du *et al.* [15] showed filament growth from the anode toward the cathode in Fe-doped $SrTiO_3$. Similarly, Yang *et al.* [8] reported oxygen vacancy drift initiating from the cathode or anode, depending on the applied bias.

V. INFLUENCE OF REACTION RATE CONSTANT

In a second study the impact of the oxygen-exchange rate on the formation and progression of the conductive filament is investigated using the continuum model. Again, an initial homogeneous donor concentration $N_{VO} = 1\times10^{16}$ cm^{-3} is assumed in the oxide layer, and no oxygen ions are assumed to be present in the Schottky-like electrode. A constant voltage pulse of 2.5 V with 1 ns rise time is applied, and the simulation is stopped after a current increase to 300 µA or more has been achieved. Fig. 2(a) shows the simulated I-t characteristics for oxygen exchange rates between $k_{00} = 1\times10^{-32}$ cm^4/s and $k_{00} = 1\times10^{-24}$ cm^4/s.

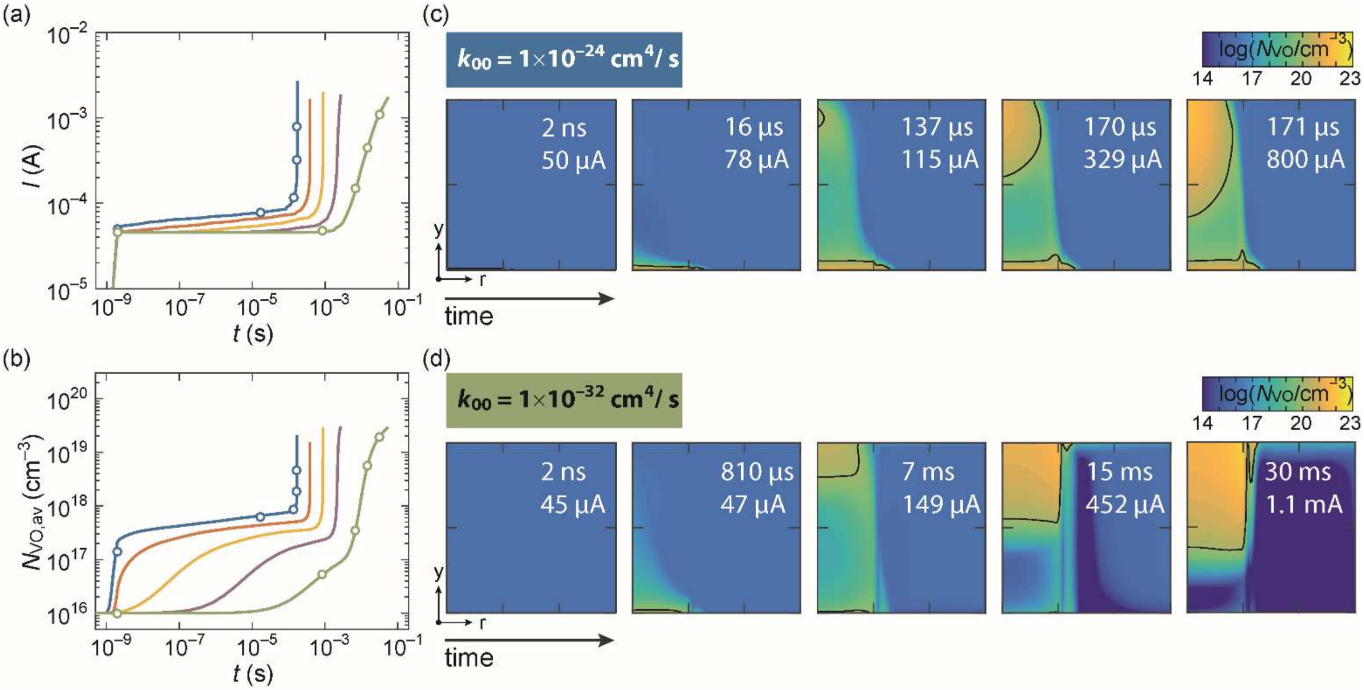

Figure 2. Simulated (a) I-t characteristics and (b) $N_{VO,av}$-t characterstics under constant voltage stress of $V_P = 2.5$ V applied to the bottom electrode of the device for different oxygen exchange rates $k_{00} = \{1\cdot10^{-24}$ cm^{-4}/s, $1\cdot10^{-26}$ cm^{-4}/s, $1\cdot10^{-28}$ cm^{-4}/s, $1\cdot10^{-30}$ cm^{-4}/s, $1\cdot10^{-32}$ cm^{-4}/s$\}$. (c) shows the evolution of the total oxygen vacancy concentration over time for $k_{00} = 1\cdot10^{-24}$ cm^{-4}/s (top row) and $k_{00} = 1\cdot10^{-24}$ cm^{-4}/s (bottom row). The snapshots correspond to the open circles in (a) and (b). The black line in the concentration maps (c), (d) marks the isoline $N_{VO} = 1\cdot10^{20}$ cm^{-3} of illustrates the filament evolution.

All current transients show a two-step process similar to the one in the previous section and as demonstrated experimentally for the SET process in RRAMs [25], [26]. This process can be explained as a thermal runaway process due to Joule heating. As in the study of the previous section, the increase in current is related to the continuous increase in oxygen-vacancy concentration in the oxide layer, which is shown in Fig. 2(b). The increase in oxygen-vacancy concentration already starts at low voltages and currents, where significant Joule heating does not yet take place. As the current increases, the associated temperature rise exerts positive feedback on the oxygen exchange rates. For large exchange rates, a thermal runaway occurs, manifesting itself in the abrupt current and concentration increase, accompanied by an abrupt increase of temperature.

The obvious influence of the oxygen exchange rate is the change of the time to form indicated by the strong increase in current. The higher the rate constant is, the faster the electroforming process is. In the present case, the time to form changes by two orders of magnitude while the rate constant changes from $k_{00} = 1\times10^{-32}$ cm^4/s to $k_{00} = 1\times10^{-24}$ cm^4/s. The oxygen-exchange current density that determines the extraction of oxygen, depends linearly on the reaction rate constant according to eq. (5). Thus, a higher exchange rate enables the faster formation of oxygen vacancies in the oxide layer, and thus a faster initial stages of the electroforming process. Once the temperature acceleration sets in, the transition occurs much faster.

The concentration maps during the electroforming process are shown in Fig. 2(c). In case of the high reaction rate constant $k_{00} = 1\cdot10^{-24}$ cm^4/s, the oxygen vacancy concentration at the bottom electrode interface is always high and the filament grows from bottom to top. In contrast, after a first increase of the oxygen vacancy concentration at 810 µs and at 7 ms, the oxygen vacancy concentration gets depleted at this interface for the low reaction rate constant, i.e., $k_{00} = 1\cdot10^{-32}$ cm^4/s. In this case, the filament growth can be considered from top to bottom. This change of the effective filament growth direction can be explained again by the interplay between oxygen vacancy generation and oxygen vacancy migration. If the oxygen rate is low, the oxygen vacancies migrate faster away from the interface than new ones are generated by the oxygen exchange reaction. Thus, the filament grows from top to bottom. If the exchange rate is high, more oxygen vacancies can be generated than are moved away from this interface resulting in a growth from bottom to top.

The exchange rate and the corresponding reduction/oxidation barrier are determined by the used electrode and oxide material, but these properties can also be influenced by the presence of hydrogen or moisture [6], [27]. Lübben et al. showed that increasing the water partial pressure in the oxide material reduces the forming voltage by several volts [28]. This observation can be related to counter reactions that happen at the electrode opposite to the one where the oxygen exchange reaction is happening. In this case, the system is kept charge neutral allowing for ionic transport. This is probably particularly important for highly insulating films where the charge is transported mainly by ions in the oxide layer. But also, for more electronically conducting films, the presence of moisture/hydrogen might reduce the barriers for the oxygen exchange reaction or lead to an increase of the reaction-rate constant.

VI. INFLUENCE OF AMBIENT CONDITIONS

Forming simulations are conducted using the 3D KMC simulation model to study the influence of the ambient temperature on the forming process. To reduce the simulation time, the oxygen vacancies (Vö) are initially placed along a filament at the center of the cell. This approach is justified as simulations with oxygen vacancies distributed throughout the entire cell exhibited similar trends. By concentrating the oxygen vacancies, computational resources can be utilized more efficiently without compromising the fundamental insights obtained.

A voltage sweep is applied starting at 0 V with a linear sweep rate of 0.5 V/s. The simulation incorporated a current compliance (*I*cc) limit of 200 µA like experiments to prevent device destruction due to uncontrolled current flow. The forming voltage (V_{Form}) is defined as the voltage at which the current compliance is reached. Upon reaching *I*cc, the simulation is terminated, and V_{Form} can be extracted.

Figure 3 illustrates a typical forming simulation performed with the 3D KMC model at $T = 300$ K. The *I-V* characteristics of the forming process (blue curve, left *y*-axis) demonstrate the linear voltage increase and the corresponding current evolution. Simultaneously, the development of the oxygen vacancy number (red curve, right *y*-axis) shows how the oxygen vacancy generation accelerates due to the increasing electric field and temperature. This self-accelerating process leads to an abrupt forming event, where the current sharply rises until *I*cc is reached. The simulation captures this dynamic and identifies the critical voltage, V_{Form}, necessary for forming. This forming process and the occurrence of a thermal runaway process is consistent with the findings of the continuum model showing the models consistency.

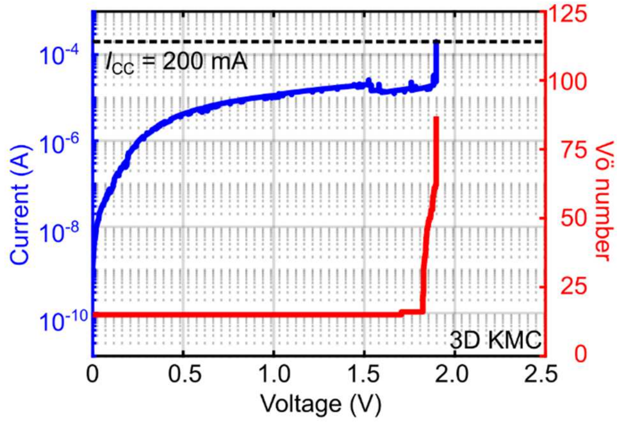

Figure 3. Forming simulation with the 3D KMC simulation model. *I-V* characteristics of the forming process of an exemplary simulation with 15 initial Vö (blue, left y-axis). The development of the oxygen vacancy (Vö) number in the cell is presented in red (right y-axis). The voltage is linearly increased with 0.5 V/s, consequently increasing the current through and the temperature in the cell. At a certain field and temperature, the generation of new oxygen vacancies at the OE starts. This increases the current, temperature, and the oxygen vacancy number in a self-accelerating process, which leads to abrupt forming. At a current compliance $I_{\mathrm{CC}} = 200$ mA the simulation is stopped, the forming is considered finished and the final voltage can be extracted and is subsequently used as forming voltage V_{Form}.

To investigate the influence of ambient conditions, the external temperature is systematically varied during the forming simulations. The temperature range could initially only be kept small, since a higher temperature increase would drastically increase the simulation time. The results reveal a slight reduction in the forming voltage (V_{Form}) with increasing ambient temperature. This trend is illustrated in Fig. 4, where the forming voltage is plotted as a function of the external temperature. Although the dataset exhibits significant scattering (blue crosses), the mean values (red line) indicate a clear negative correlation between the ambient temperature and V_{Form}. The observed decrease in V_{Form} can be attributed to the enhanced thermal energy at elevated temperatures, which facilitates the generation and migration of oxygen vacancies, thus reducing the electric field required for the forming process. This trend is consistent with experimental data obtained on HfO_2-based ReRAM [28]. Butcher *et al.* [28] found that higher temperatures enhance electron transfer and oxygen vacancy generation, enabling forming at lower voltages. This approach also improves device uniformity and significantly reduces forming time, making it more practical for industrial applications.

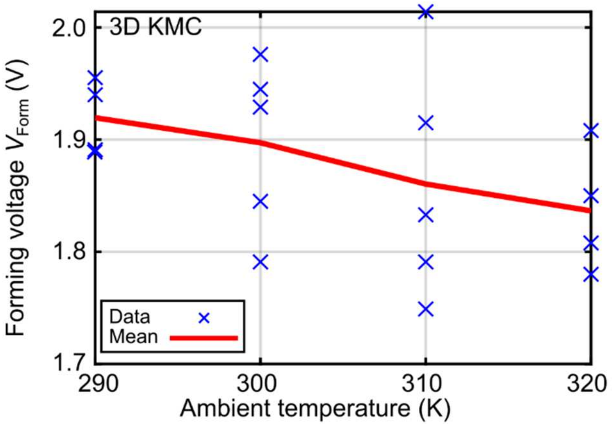

Figure 4. Dependence of the forming voltage V_{Form} on the ambient temperature of the VCM cell. Despite the limited statistics and the comparably high scattering of the data points (blue crosses), a small decrease of the forming voltage V_{Form} with increasing ambient temperature can be observed looking at the mean values (red line).

VII. INFLUENCE OF DEFECT CONCENTRATION

In this section, forming simulations are conducted to examine the impact of the initial number of oxygen vacancies in the oxide layer on the forming process. Unlike the previous chapter, where simulations were performed at various ambient temperatures, all simulations here are conducted at a constant temperature of 300 K. To optimize computational efficiency, the oxygen vacancies are initially placed along a filament at the center of the cell, as described earlier.

By systematically varying the initial oxygen vacancy number, the simulations aim to uncover how the number of pre-existing oxygen vacancies influences the dynamics of the

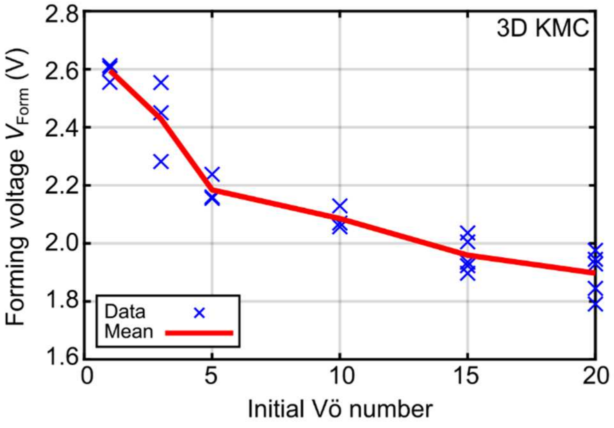

Figure 5. Dependence of the forming voltage V_{Form} on the initial number of oxygen vacancies (Vö) in the HfO_x-layer of the VCM cell. With an increasing initial oxygen vacancy number, the forming voltage decreases.

forming process and especially the forming voltage (V_{Form}). The forming simulations are carried out by varying the initial number of Vö in the oxide layer from 1 to 20. For each simulation, the corresponding V_{Form} is extracted and plotted as a function of the initial Vö concentration in Fig. 5. The results reveal a clear inverse relationship between these two quantities: as the initial number of oxygen vacancies increases, the forming voltage decreases approaching typical SET voltages. This behavior can be attributed to the enhanced electrical conductivity of the system with a higher initial oxygen vacancy concentration. The increased oxygen vacancy density allows a higher current flow through the cell, resulting in elevated system temperatures. Consequently, the critical processes for forming, such as the generation of new oxygen vacancies, are triggered at lower voltages. This trend has been also observed in experiments [3], [4], [5], [29]. Piros *et al.* [3] found that high oxygen vacancy density in Y_2O_3 enables forming-free behavior, while Sharath *et al.* [4] showed that oxygen-deficient TaO_x reduces forming voltages. Stille *et al.* [5] similarly observed that higher defect densities in $SrTiO_3$ lower forming voltages by promoting localized reduction processes.

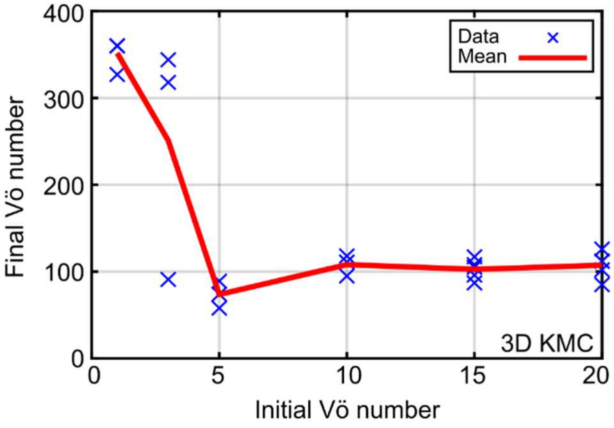

Figure 6. Final number of oxygen vacancies (Vö) in the cell after I_{CC} is reached and the forming is finished in dependence of the initially placed number of Vö. It can be observed that the final Vö number is clearly higher for very low initial Vö numbers, whereas the final Vö number stays relatively constant for higher initial Vö numbers.

In the next step, the final number of oxygen vacancies in the system – i.e., the number of oxygen vacancies present as the current compliance is reached – was extracted from the forming simulations. Figure 6 illustrates the relationship between the final oxygen vacancy number and the initial oxygen vacancy number. For low initial oxygen vacancy concentrations, the final oxygen vacancy number is significantly higher, indicating substantial oxygen vacancy generation during the forming process. Conversely, for higher initial oxygen vacancy concentrations, the final number of oxygen vacancies remains relatively constant, suggesting that the system is approaching a saturation regime where the forming process generates fewer additional oxygen vacancies.

Additionally, the final number of oxygen vacancies was plotted against the corresponding forming voltage (V_{Form}), as shown in Fig. 7. This analysis reveals that the final oxygen vacancy number increases with higher V_{Form}. This trend can be interpreted as follows: at higher forming voltages, the critical processes – such as the generation and migration of oxygen vacancies – occur under stronger electric fields. This results in rapid and substantial oxygen vacancy generation within a short time span. In contrast, at lower V_{Form}, the processes of oxygen vacancy generation and diffusion towards the active electrode are better balanced. This balance leads to the formation of a more ordered filament structure that facilitates current flow. Conversely, higher forming voltages produce a less ordered, oxygen vacancy-rich system, which may negatively impact filament stability and uniformity.

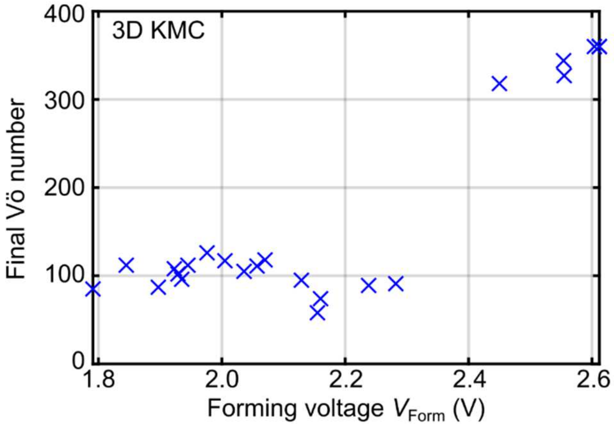

Figure 7. Final number of oxygen vacancies (Vö) in the cell as a function of the forming voltage V_{Form}. Higher forming voltages result in a greater number of final oxygen vacancies due to accelerated oxygen vacancy generation at elevated electric fields.

Finally, in Fig. 8 two exemplary oxygen vacancy configurations resulting from the forming simulations are presented. The final spatial distribution of the oxygen vacancy represented by red spheres in the oxide of the VCM ReRAM cell after the forming process and reaching the current compliance I_{CC} is presented for two different cases. In Fig. 8 a), an example of a cell with a low initial oxygen vacancy number (3 Vö) and correspondingly a high forming voltage (V_{Form} = 2.54 V) is shown. As mentioned before, the generation of oxygen vacancies is dominating here at the time the forming starts, leading to a high final number of oxygen vacancies (336) without building a complete filament. In contrast, in Fig. 8 b)

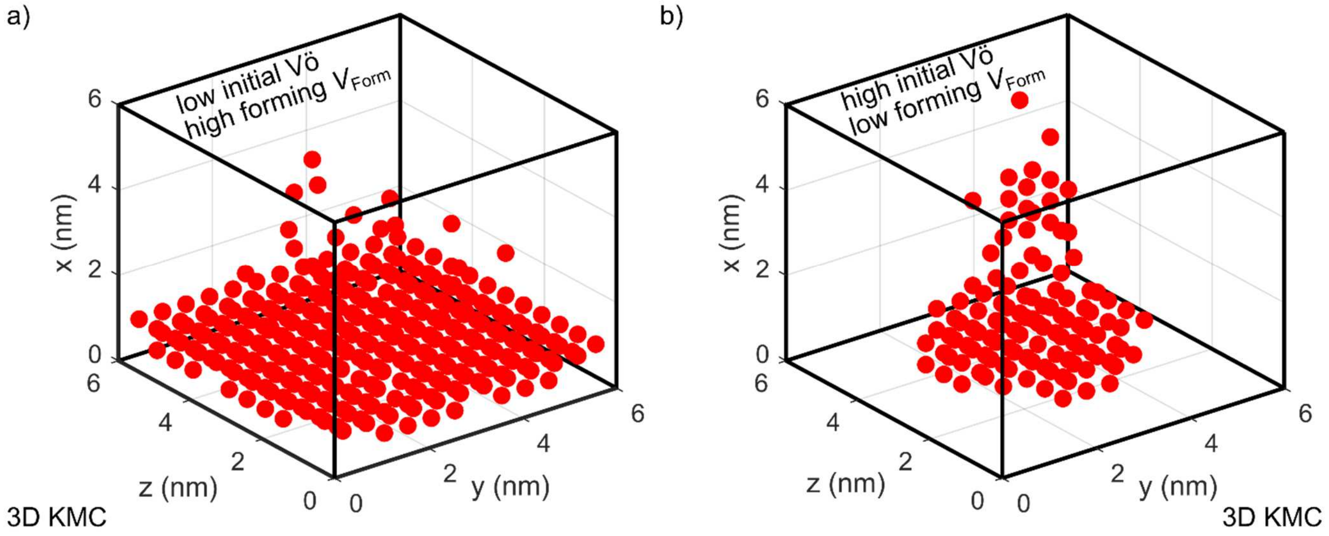

Figure 8. Exemplary spatial representation of the Vö (red spheres) in the oxide of the VCM ReRAM cell after completion of forming by achieving the current compliance limit I_{CC}. a) Low initial Vö number (3 Vö) leading to a late forming process at a high voltage of $V_{Form} = 2.54$ V. Vö generation strongly dominates, leading to a high final number of Vö (336) with only partially formed filament. b) Higher initial Vö number (15 Vö) leading to an earlier forming process at a lower voltage of $V_{Form} = 2.02$ V. Vö generation and drift-diffusion towards active top electrode are more balanced leading to a well-formed filament with 98 final Vö.

the example of a cell with 15 initial oxygen vacancies and a corresponding forming voltage of $V_{Form} = 2.02$ V is shown. Here, the generation of oxygen vacancies is more balanced with the drift-diffusion of the oxygen vacancies towards the top electrode, leading to a well-formed filament.

VIII. SUMMARY

In this work, some of the parameters determining the electroforming of metal/oxide/metal stacks are investigated using simulations. It is shown that the forming voltage/time to form decreases if the voltage is increased, the reaction constant increases, the number of initial defects increases, or the temperature increases. This is consistent with experimental findings. Moreover, it is shown that the parameters not only influence the forming voltage/time to form but also impact the shape of the formed filament.

ACKNOWLEDGMENT

The authors gratefully acknowledge computing time on the supercomputer JURECA [30] at Forschungszentrum Jülich under grant no. 27525.

REFERENCES

[1] R. Dittmann, S. Menzel, and R. Waser, “Nanoionic memristive phenomena in metal oxides: the valence change mechanism,” *Adv Phys.*, vol. 70, no. 2, pp. 155–349, 2021, doi: 10.1080/00018732.2022.2084006.

[2] A. Padovani, L. Larcher, G. Bersuker, and P. Pavan, “Charge Transport and Degradation in HfO_2 and HfO_x Dielectrics,” *IEEE Electron Device Lett.*, vol. 34, no. 5, pp. 680–682, 2013, doi: 10.1109/LED.2013.2251602.

[3] E. Piros *et al.*, “Role of Oxygen Defects in Conductive-Filament Formation in Y2O3-Based Analog RRAM Devices as Revealed by Fluctuation Spectroscopy,” *Phys. Rev. Appl.*, vol. 14, no. 3, p. 34029/1–7, 2020, doi: 10.1103/PhysRevApplied.14.034029.

[4] S. U. Sharath *et al.*, “Impact of oxygen stoichiometry on electroforming and multiple switching modes in TiN/TaO_x/Pt based ReRAM,” *Appl. Phys. Lett.*, vol. 109, no. 17, p. 173503/1–5, 2016, doi: 10.1063/1.4965872.

[5] S. Stille *et al.*, “Detection of filament formation in forming-free resistive switching $SrTiO_3$ devices with Ti top electrodes,” *Appl. Phys. Lett.*, vol. 100, no. 22, p. 223503/1–4, 2012, doi: 10.1063/1.4724108.

[6] M. Lübben, S. Wiefels, R. Waser, and I. Valov, “Processes and Effects of Oxygen and Moisture in Resistively Switching TaO_x and HfO_x,” *Adv. Electron. Mater.*, vol. 4, no. 1, p. 1700458, 2018, doi: 10.1002/aelm.201700458.

[7] K. Szot, W. Speier, G. Bihlmayer, and R. Waser, “Switching the electrical resistance of individual dislocations in single-crystalline $SrTiO_3$,” *Nat. Mater.*, vol. 5, no. 4, pp. 312–320, 2006, doi: 10.1038/nmat1614.

[8] J. J. Yang *et al.*, “The mechanism of electroforming of metal oxide memristive switches,” *Nanotechnology*, vol. 20, no. 21, p. 215201, 2009, doi: 10.1088/0957-4484/20/21/215201.

[9] M. Buckwell *et al.*, “Microscopic and spectroscopic analysis of the nature of conductivity changes during resistive switching in silicon-rich silicon oxide,” *Phys. Status Solidi C*, vol. 12, pp. 211–217, 2015, doi: 10.1002/pssc.201400160.

[10] M. Sowinska *et al.*, “Hard x-ray photoelectron spectroscopy study of the electroforming in Ti/HfO_2-based resistive switching structures,” *Appl. Phys. Lett.*, vol. 100, p. 233509, 2012, doi: 10.1063/1.4728118.

[11] J. Kwon, A. A. Sharma, J. A. Bain, Y. N. Picard, and M. Skowronski, “Oxygen Vacancy Creation, Drift, and Aggregation in TiO_2-Based Resistive Switches at Low Temperature and Voltage,” *Adv. Funct. Mater.*, vol. 25, no. 19, pp. 2876–2883, 2015, doi: 10.1002/adfm.201500444.

[12] D.-H. Kwon *et al.*, “Atomic structure of conducting nanofilaments in TiO2 resistive switching memory,” *Nat. Nanotechnol.*, vol. 5, no. 2, pp. 148–153, 2010, doi: 10.1038/NNANO.2009.456.

[13] C. Linderälv, A. Lindman, and P. Erhart, “A Unifying Perspective on Oxygen Vacancies in Wide Band Gap Oxides,” *J. Phys. Chem. Lett.*, vol. 9, no. 1, pp. 222–228, 2018, doi: 10.1021/acs.jpclett.7b03028.

[14] C. Funck and S. Menzel, “Comprehensive Model of Electron Conduction in Oxide-Based Memristive Devices,” *ACS Appl. Electron. Mater.*, vol. 3, pp. 3674–3692, 2021, doi: 10.1021/acsaelm.1c00398.

[15] H. Du *et al.*, “Nanosized conducting filaments formed by atomic-scale defects in redox-based resistive switching memories,” *Chem. Mater.*, vol. 29, pp. 3164–3173, 2017, doi: 10.1021/acs.chemmater.7b00220.

[16] C. Baeumer *et al.*, "Subfilamentary Networks Cause Cycle-to-Cycle Variability in Memristive Devices," *ACS Nano*, vol. 11, no. 7, pp. 6921–6929, 2017, doi: 10.1021/acsnano.7b02113.

[17] E. Abbaspour, "Modeling and simulation of valence-change based resistive switching," 2019.

[18] N. Kopperberg, S. Wiefels, S. Liberda, R. Waser, and S. Menzel, "A Consistent Model for Short-Term Instability and Long-Term Retention in Filamentary Oxide-Based Memristive Devices," *ACS Appl. Mater. Interfaces*, vol. 13, no. 48, pp. 58066–58075, 2021, doi: 10.1021/acsami.1c14667.

[19] S. Wiefels *et al.*, "Reliability Aspects of 28nm BEOL-Integrated Resistive Switching Random Access Memory," *Phys. Status Solidi A*, p. 2300401, 2023, doi: 10.1002/pssa.202300401.

[20] A. Marchewka *et al.*, "Nanoionic Resistive Switching Memories: On the Physical Nature of the Dynamic Reset Process," *Adv. Electron. Mater.*, vol. 2, no. 1, p. 1500233/1–13, 2016, doi: 10.1002/aelm.201500233.

[21] A. Marchewka, R. Waser, and S. Menzel, "Physical Modeling of the Electroforming Process in Resistive-Switching Devices," 2017, pp. 133–136. doi: 10.23919/SISPAD.2017.8085282.

[22] C. Funck *et al.*, "Comprehensive model for the electronic transport in Pt/$SrTiO_3$ analog memristive devices," *Phys. Rev. B Condens. Matter*, vol. 102, p. 035307, 2020, doi: 10.1103/PhysRevB.102.035307.

[23] M. Lübben, "Redox Processes at Interfaces and Ionic Motion in Resistively Switching Materials," 2020.

[24] E. Yalon, I. Karpov, V. Karpov, I. Riess, D. Kalaev, and D. Ritter, "Detection of the insulating gap and conductive filament growth direction in resistive memories," *Nanoscale*, vol. 7, no. 37, pp. 15434–15441, 2015, doi: 10.1039/c5nr03314d.

[25] K. Fleck, C. La Torre, N. Aslam, S. Hoffmann-Eifert, U. Böttger, and S. Menzel, "Uniting Gradual and Abrupt SET Processes in Resistive Switching Oxides," *Phys. Rev. Appl.*, vol. 6, no. 6, p. 064015, 2016, doi: 10.1103/PhysRevApplied.6.064015.

[26] F. Cüppers *et al.*, "Exploiting the switching dynamics of HfO2-based ReRAM devices for reliable analog memristive behavior," *Appl. Phys. Lett. Mater.*, vol. 7, no. 9, p. 091105/1–9, 2019, doi: 10.1063/1.5108654.

[27] Y. Y. Chen *et al.*, "Hydrogen-Induced Resistive Switching in TiN/ALD HfO2/PEALD TiN RRAM Device," *IEEE Electron Device Lett.*, vol. 33, pp. 483–485, 2012, doi: 10.1109/LED.2012.2185212.

[28] B. Butcher *et al.*, "Hot Forming to Improve Memory Window and Uniformity of Low-power HfO_x-based RRAMs," 2012, p. 4 pp.-4 pp. doi: 10.1109/IMW.2012.6213647.

[29] K. Skaja, M. Andrae, V. Rana, R. Waser, R. Dittmann, and C. Baeumer, "Reduction of the forming voltage through tailored oxygen non-stoichiometry in tantalum oxide ReRAM devices," *Sci. Rep.*, vol. 8, p. 10861/1–7, 2018, doi: 10.1038/s41598-018-28992-9.

[30] P. Thoernig, "JURECA: Data Centric and Booster Modules implementing the Modular Supercomputing Architecture at J{ue}lich Supercomputing Centre," *J. Large-Scale Res. Facil. JLSRF*, vol. 7, pp. A182–A182, 2021.